



Article

# Effects of Freeze-Thaw and Wet-Dry Cycles on Tension Stiffening Behavior of Reinforced RAC Elements

Caroline Santana Rangel <sup>1</sup>, Marco Pepe <sup>2,3</sup>, Mayara Amario <sup>1,4</sup>, Lucas Caon Menegatti <sup>1</sup>, Enzo Martinelli <sup>2,3</sup>  
and Romildo Dias Toledo Filho <sup>1,\*</sup>

- <sup>1</sup> Department of Civil Engineering, COPPE, Federal University of Rio de Janeiro, Rio de Janeiro 21945970, Brazil; carolrangel@poli.ufrj.br (C.S.R.); mayara@coc.ufrj.br (M.A.); lucas.menegatti@coc.ufrj.br (L.C.M.)
- <sup>2</sup> Department of Civil Engineering, University of Salerno, 84084 Fisciano, Italy; ma pepe@unisa.it (M.P.); e.martinelli@unisa.it (E.M.)
- <sup>3</sup> TESIS srl, 84084 Fisciano, Italy
- <sup>4</sup> Department of Civil Construction, POLI, Federal University of Rio de Janeiro, Rio de Janeiro 21941909, Brazil
- \* Correspondence: toledo@coc.ufrj.br

**Abstract:** In the last several decades, the growth of Construction and Demolition Waste (CDW) production and the increased consumption of natural resources have led to promoting the use of secondary raw materials for a more sustainable construction. Specifically, the use of Recycled Concrete Aggregate (RCA), derived from waste concrete, for the production of Recycled Aggregate Concrete (RAC) has attracted a significant interest both in industry and in academia. However, the use of RAC in field applications still finds some barriers. In this context, the present study investigates experimentally the effects of freeze-thaw and wet-dry cycles on the stress transfer mechanisms of reinforced RAC elements through tension stiffening tests. First of all, the paper presents a detailed analysis of the degradation due to the aging process of RAC with RCAs obtained from different sources. Particularly, the results of tension stiffening tests are analyzed in terms of crack formation and propagation, matrix tensile strength contribution and steel-to-concrete bond. The results highlight that the pre-cracking elastic modulus, the first crack strength as well as the maximum concrete strength are strongly influenced by the presence of the Attached Mortar (AM) in RCA, as the former affects the concrete's open porosity. Therefore, the amount of AM is identified as the key parameter for the evaluation of durability of reinforced RAC members: a degradation-law is also proposed which correlates the initial concrete open porosity with the damage observed in reinforced RAC elements.

**Keywords:** Recycled Concrete Aggregate (RCA); Recycled Aggregate Concrete (RAC); reinforced concrete; tension stiffening; durability; freeze-thaw cycles; wet-dry cycles; open porosity



**Citation:** Santana Rangel, C.; Pepe, M.; Amario, M.; Menegatti, L.C.; Martinelli, E.; Toledo Filho, R.D. Effects of Freeze-Thaw and Wet-Dry Cycles on Tension Stiffening Behavior of Reinforced RAC Elements. *Appl. Sci.* **2021**, *11*, 10063. <https://doi.org/10.3390/app112110063>

Academic Editors: Jorge de Brito and João Pacheco

Received: 23 September 2021  
Accepted: 22 October 2021  
Published: 27 October 2021

**Publisher's Note:** MDPI stays neutral with regard to jurisdictional claims in published maps and institutional affiliations.



**Copyright:** © 2021 by the authors. Licensee MDPI, Basel, Switzerland. This article is an open access article distributed under the terms and conditions of the Creative Commons Attribution (CC BY) license (<https://creativecommons.org/licenses/by/4.0/>).

## 1. Introduction

The continuous development of the construction and infrastructure sectors has become a global concern in regards to sustainability issues, due to the high consumption of non-renewable natural resources as raw materials and the massive production of Construction and Demolition Waste (CDW). The use of CDW to produce Recycled Concrete Aggregate (i.e., RCA identifying recycled aggregate obtained from concrete debris) can be an effective way to mitigate these negative environmental impacts [1–3].

The main difference between Recycled Concrete Aggregate (RCA) and Natural Aggregate (NA) relies on the presence of the existing Attached Mortar (AM) layer on the recycled aggregate surface, and, consequently, the presence of an Interfacial Transition Zone (ITZ) between AM and original aggregate [4,5]. An investigation carried out by Verian et al. [4] showed that AM makes the RCA a more porous material compared to NA. As a consequence, RCA presents lower value of specific gravity and higher water absorption capacity,

apart from typically higher value of L.A. abrasion wear [4,6]. Despite this, Amario et al. [7] verified the feasibility of producing normal and high strength Recycled Aggregate Concrete (i.e., RAC identifying concrete mixture produced with recycled aggregates) without compromising mechanical properties by using the Compressible Packing Model (CPM) for the rational proportioning of RAC mixtures. However, the use of RCA in the construction sector is not widely accepted and it is often limited to non-structural applications [8].

Besides the mechanical performance, durability is one of the main requirements for concrete structures, as they are widely exposed to environmental attacks, but should guarantee the requested safety levels during their entire life service. In fact, degradation mechanisms are usually driven by the exposure to environmental conditions, such as temperature and relative humidity variations and the availability of ions and deleterious agents [9]. The most common attacks that compromise durability of reinforced concrete structures are corrosion of steel, freeze-thaw damage, sulfate and chloride attack, salt scaling, and alkali aggregates reactions [10]. As a common consequence, all these attacks can result in cracking and spalling of the reinforced concrete surfaces, intensifying the degradation processes. Within this context, some studies have been carried out to investigate the steel-concrete bond behavior under the action of environmental factors and, in this general context, this paper focused on the degradation processes of reinforced Recycled Aggregate Concrete (RAC) due to the effects of freeze-thaw and wet-dry cycles.

Since freeze-thaw cycles reduce concrete strength, change the internal pore structure and cause the appearance of cracks, they also influence the bond between steel and concrete, which can affect structural performance [11,12]. The damage caused to the structure by repeated freeze-thaw cycles varies from the surface fragmentation to complete concrete disintegration. However, the damage caused by this phenomenon can be minimized by reducing the capillary pores volume in the concrete with, for example, a lower  $w/c$  ratio or using suitable admixtures [13–16].

Rangel et al. [17] investigated durability of both normal- (C35) and high-strength (C60) RACs produced with RCAs derived from different sources and subjected to different numbers of freeze-thaw cycles (0, 150, and 300). The results showed that the degradation mainly affected the concrete mortar. For the high-strength RAC, the attached mortar was the fragile phase, while on the normal-strength RAC, the new mortar was the one which did not resist the internal efforts generated by the cycles. The degradation cycles had a higher impact on the mechanical and physical performances of normal strength concretes than the high strength mixtures. Nevertheless, all concrete mixtures showed a reduction in the compressive and tensile strength, as well as in the concrete mass. The presence of RCAs increased the porosity of the concrete and, consequently, decreased the freeze-thaw durability of RACs.

Some researchers [18–20] conducted pull-out tests to investigate the bond behavior between RAC and steel bars after freeze-thaw cycles. Ren et al. [18] found that the bond strength of steel-RAC decreases as the freeze-thaw cycles increase: the interface between the steel bar and the concrete deteriorates with the cycles, the formation and propagation of interfacial cracks occurs and the chemical bond between the steel bar and the concrete is reduced. According to Shang et al. [19], the bond behavior reduction with freeze-thaw cycles was more pronounced for plain steel than for deformed steel bars. As for the latter, the bond strength tends to decrease as the diameter of the bar increases.

Huaishuai et al. [20] highlighted that as concrete subjected to freeze-thaw cycles deteriorates, the frictional force and the mechanical force between bar and concrete are weakened and, hence, the bond strength is reduced. Additionally, the researchers noticed that there was a greater reduction in steel-RAC bond by increasing the number of cycles. In general, freeze-thaw damage occurs in the concrete due to its porosity. When freezing, water exhibits an expansive behavior and, if the volume available in the pores is not sufficient and the pressure exerted by ice exceeds the strength of the material, micro-cracks can be formed in concrete.

In the wetting and drying process, evaporation of water from the pores during the drying stage causes shrinkage and micro-cracks in the concrete. When experiencing another wetting stage, the microstructure recovers water and swells; however, some of the changes that occurred in the previous drying stage are not reversible. The periodicity of this cyclical process leads to cracking and fragmentation of the concrete surface [21].

Rangel et al. [22] analyzed the physical and mechanical performance of structural concrete made with either natural or recycled aggregates after exposure to wet-dry cycles. The investigation results revealed that the degradation of RAC was greater than in natural concretes, mainly after a high number of cycles. It is believed that this occurs because of the presence of AM, so that RAC presents fragmentation in both the new mortar and the old mortar attached to the RCA particles, suffering, therefore, greater damages than natural concrete, which undergoes the degradation process only in the new mortar. The researchers also concluded that RAC resistance to wet-dry degradation is governed by the initial open porosity of the concrete.

Despite advances in research on RAC, there is little data on steel-concrete performance after aging. Therefore, the present paper presents the results of an experimental study aimed at assessing structural durability by analyzing tension stiffening performance, crack propagation, isolated matrix capacity and steel-RAC bond after exposing the reinforced elements to degradation processes, i.e., freeze-thaw and wet-dry cycles.

## 2. Materials and Methods

### 2.1. Materials

#### 2.1.1. Raw Materials

Coarse Recycled Concrete Aggregate (RCA) were produced from two different sources (more details in Rangel et al. [23]): one derives from a laboratory-produced concrete waste, labeled “L-waste”, and the other comes from a concrete waste provided by a demolition waste recycling plant, labeled “D-waste”. The residues were subjected to the same processing steps (crushing, mechanical sieving, homogenization and drying) for the production of the RCAs, labeled “RCA\_L\_C1” and “RCA\_D\_C1”. As Natural Coarse Aggregate (NCA), granite-type rocks were used in two sizes, named “NCA\_C0” and “NCA\_C1”. As Natural Fine Aggregate (NFA), natural quartz sand was used. Table 1 presents the characterization of the aggregates. Meanwhile, Figure 1 presents the grain size distribution of natural and recycled aggregates. The data summarized in Table 1 show that the recycled particles are characterized by a significant higher water absorption capacity and lower density in comparison with the companion (i.e., same class size) natural aggregates while the grain size distribution is quite similar (see Figure 1).

As for cement, an “high initial strength Portland cement” (labeled CPV-ARI, according to the National Brazilian Standard [27]) with specific gravity of 3181 kg/m<sup>3</sup> and 28-day compressive strength of 40.6 MPa was used. As additive, a polycarboxylate superplasticizer (labeled MC Powerflow 1180) with specific gravity of 1070 kg/m<sup>3</sup>, solid concentration content of 35% and saturation dosage of 1.5% (solids of SP based on the cement weight) was used.

**Table 1.** Properties of the natural and recycled aggregates used (Rangel et al. [23]).

| Properties                                    | NFA  | NCA_C0 | NCA_C1 | RCA_L_C1 | RCA_D_C1 |
|---|------|--------|--------|----------|----------|
| D <sub>max</sub> (mm)                         | 4.75 | 9.5    | 19.0   | 19.0     | 19.0     |
| Specific gravity (kg/m <sup>3</sup> ) [24,25] | 2447 | 2662   | 2636   | 2105     | 2255     |
| Water absorption (%) [24,25]                  | 0.5  | 1.5    | 1.3    | 8.2      | 6.1      |
| Attached Mortar—V <sub>AM</sub> (%) [23]      | -    | -      | -      | 64.8     | 35.1     |
| Abrasion wear (%) [26]                        | -    | 39.5   | 36.1   | 46.7     | 46.3     |

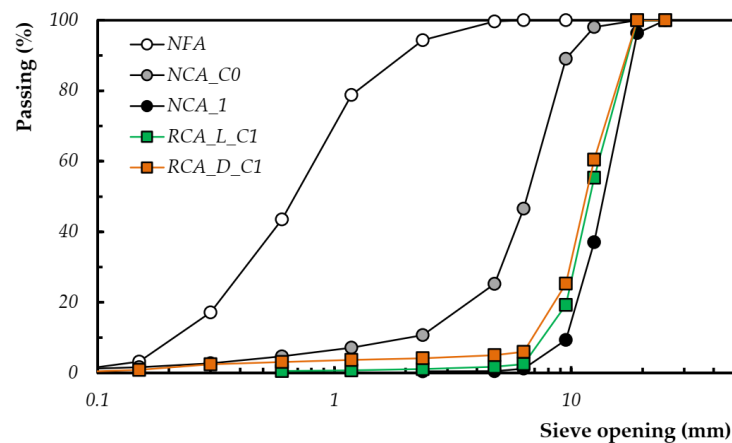


Figure 1. Grain size distribution of natural and recycled aggregates.

### 2.1.2. Natural and Recycled Aggregate Concrete

The mixture proportioning for the concretes analyzed as part of this study was based on the Compressible Packing Model (CPM), proposed by de Larrard [28]. The original CPM assumes that, during mixing, the aggregates are in a dry condition and their water absorption capacity at 24 h should be considered by introducing additional water for their saturation. However, as also reported in Table 2, the RCAs are generally characterized by a significantly higher water absorption capacity compared to that of natural aggregates. Recent studies [29] demonstrated that they are not able to absorb such amount of water during the mixing time and, as a consequence, some extra water in the mixture could cause an increase in the effective water-cement ratio [30]. For this reason, in the present study the produced mixtures were prepared in accordance with the methodology proposed by Amario et al. [7]: the RCAs are employed in fully dried condition and 50% of their water absorption capacity is considered for saturation during mixing.

Table 2. Mix proportions and main properties of NAC and RACs used (Rangel et al. [17]).

| Mixtures                       | C35-NAT                               | C35-L-C1 | C35-D-C1 |      |
|--------------------------------|---------------------------------------|----------|----------|------|
| Materials (kg/m <sup>3</sup> ) | NCA_C1                                | 452      | 0        | 0    |
|                                | RCA_L_C1                              | 0        | 361      | 0    |
|                                | RCA_D_C1                              | 0        | 0        | 384  |
|                                | NCA_C0                                | 457      | 456      | 453  |
|                                | NFA                                   | 868      | 867      | 862  |
|                                | Cement                                | 325      | 336      | 341  |
|                                | SP                                    | 1.86     | 1.92     | 1.95 |
|                                | Effective water                       | 196      | 191      | 194  |
|                                | Total water                           | 212      | 216      | 216  |
| Mixture parameters             | Effective <i>w/c</i>                  | 0.60     | 0.57     | 0.57 |
|                                | Total mortar volume (%)— $V_{M,tot}$  | 65.5     | 77.6     | 73.1 |
| 28-days properties             | Water absorption (%) [31]— $w_{open}$ | 3.0      | 3.9      | 3.5  |
|                                | $f_{c,28}$ (MPa) [32]                 | 34.2     | 35.3     | 33.5 |
|                                | $E_{c,28}$ (GPa) [33]                 | 21.3     | 21.2     | 20.9 |
|                                | $f_{t,28}$ (MPa) [34]                 | 2.7      | 2.9      | 2.6  |

The use of this mix-design method represents one of the key novelty of the present research since, as also well demonstrated by the authors in the literature [7,22], it allows the production of recycled and natural concrete characterized by the same strength class, by considering the specific features of the employed raw materials. Thus, individual mix-design was previously developed for each mixture (for more details see Rangel et al. [17]), so that the simple replacement (in mass or volume, generally adopted in the literature) of the natural aggregate by RCA in the reference mixture was not carried out.

For the experimental investigation of the present study, three normal-strength concrete mixtures were used, with 28-days main properties already known, as shown in Table 2. The choice of producing normal-strength (i.e., C35) mixtures was based on the fact that when high-strength RAC mixtures are produced, the potential detrimental effect of RCA on the resulting RAC durability is mitigated by the low porosity of the cementitious matrix [17,22].

Table 2 also reports (in the mixture parameter rows) the amount of total mortar volume ( $V_{M,tot}$ ), which represents a relevant parameter for RAC mixtures. In fact, it is determined by the sum of the volume of the attached mortar ( $V_{AM}$ ) present in RCAs (Table 1) and the new mortar volume given by the sum of sand, cement, water and superplasticizer present within the mixture [17,22]. In addition, as demonstrated by the authors in previous studies [17,22], the water absorption capacity of the hardened mixture at 28 days (i.e.,  $w_{open}$  in Table 2) is strictly related to the total mortar volume by the following equation:

$$w_{open} = \frac{k_1 \cdot (V_{M,tot} - V_{M,0})}{k_2 + (V_{M,tot} - V_{M,0})} \quad (1)$$

where  $k_1$  (equal to 7.30)  $k_2$  (equal to 30) and  $V_{M,0}$  (equal to 45) represent constant values that were calibrated for the C35 in previous studies [17,22].

### 2.1.3. Steel Bars

Deformed steel bars of CA-50 type, with a diameter of 12.5 mm, were used as reinforcement, with the following characterization [35]: yield force of 67.3 kN, yield strength of 540 MPa, ultimate strength of 680 MPa and elastic modulus of 198 GPa.

## 2.2. Methods

### 2.2.1. Production of Reinforced Elements

Prismatic reinforced concrete specimens were produced as shown in Figure 2. Initially, a layer of oil was applied to the molds to facilitate the demolding process and the steel bars were fixed. For the mixing procedure, due to the high absorption of RCAs, the specific methodology of the two-stage mixing approach (TSMA) [36,37], developed and improved for concrete containing RCAs, was adopted. The casting of the concrete was carried out in two layers, followed by mechanical compaction. The elements were demolded after 24 h and conducted to cure in wet chamber (relative humidity of 100% and temperature of 21 °C).

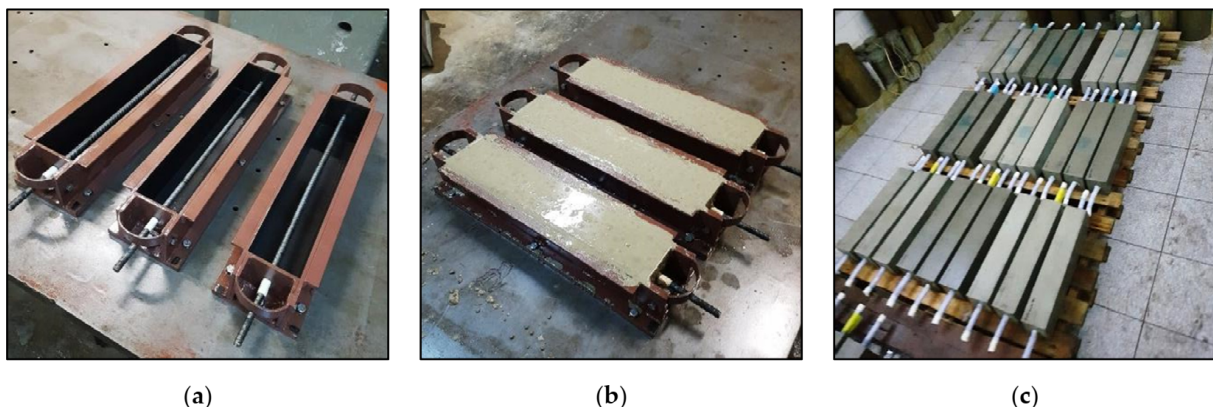


**Figure 2.** Production of reinforced elements: (a) Preparation; (b) Casting; (c) Curing.

### 2.2.2. Freeze-Thaw and Wet-Dry Aging Procedures

The aging procedures were started after 28 days of curing. Initially, the specimens were kept immersed in water at a temperature of 20 °C for 48 h. Then, three prismatic specimens of each mixture were subjected to each type of degradation test as explained:

- Freeze-thaw cycles (FTC): the samples were submitted to 0, 150 and 300 accelerated freezing and thawing cycles, based on ASTM C666 [38], in a climatic chamber with an automatic temperature control system. The total time of one cycle was 5 h, with a temperature reduction from 4 °C to −18 °C in 2.5 h and then reheating for 2.5 h until reaching 4 °C again;
- Wet-dry cycles (WDC): the samples were submitted to 0, 25 and 50 accelerated wetting and drying cycles, based on NBR 13554 [39] and ASTM D559 [40], and it was performed manually with the use of a water tank and a laboratory oven. The total time of one cycle was 24 h, which consisted of immersion in water at 20 °C for 3 h, superficial drying at 21 °C for 1 h and oven-drying at 60 °C for 20 h.
- In addition, non-degraded samples were kept in a wet chamber and tested as reference at the same age as the degraded samples.

### 2.2.3. Tension Stiffening Test

Figure 3 presents the specimen dimensions and the test set-up. The specimen of the tension stiffening test consists of a concrete prism reinforced with a single centralized steel rebar: with cross section of  $95 \times 95 \text{ mm}^2$ , bond length of 500 mm and steel bar of 12.5 mm diameter and 760 mm length. Before the test, the surfaces of the specimens were painted with a mixture of water and white paint, to allow a better visualization of the appearance of cracks. The test was adapted from NBR 7477 [41] and performed with a constant speed of 0.3 mm/min. The tests were carried out in three specimens, and the force-strain behavior was obtained with the use of two electrical transducers (LVDTs) attached on both specimen sides.

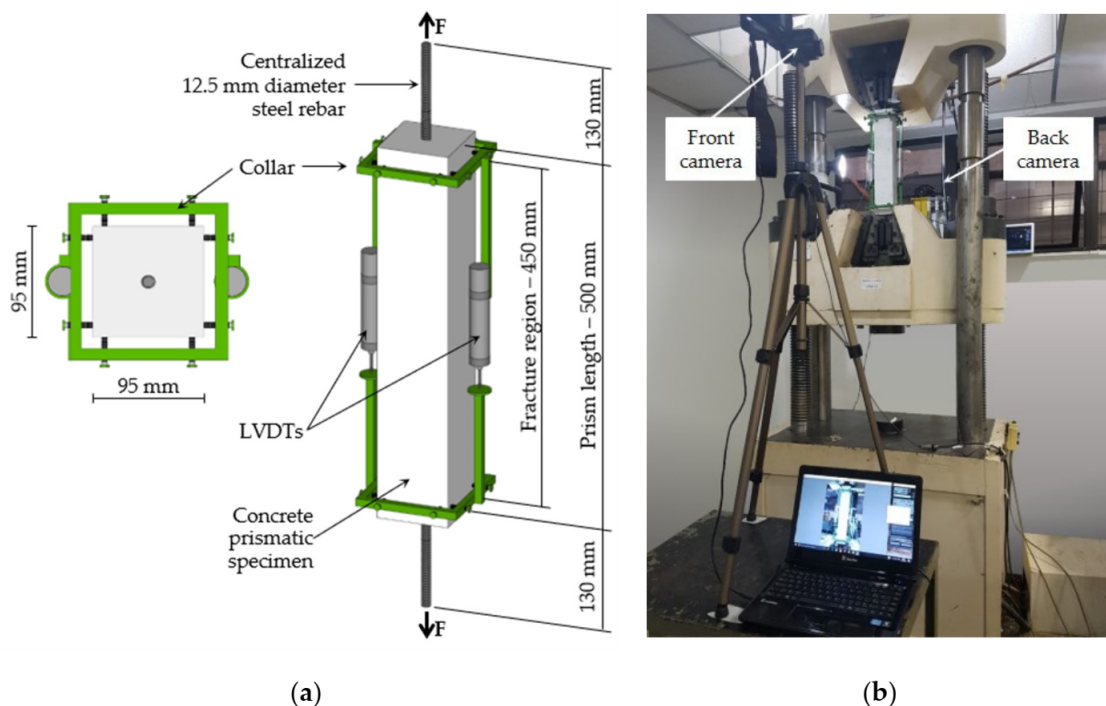


**Figure 3.** Tension stiffening test: (a) Specimen dimensions; (b) Test set-up.

### 2.2.4. Crack Analysis Method

Photos of the details of the cracking process were recorded at different stages of deformation/force (Figure 3b). In other words, the study of crack propagation in the tension stiffening test was carried out based on image analysis. The images throughout the tests were captured with a high resolution digital camera, at intervals of 30 s, kept in the same position from the beginning to the end of the test. To calculate the average spacing between cracks, five readings were taken from each region, and the mean value for each

deformation considered is referred to as “crack spacing”. In order to calculate the crack opening, ten readings were made in each deformation considered, and the final average crack opening value is referred to as “crack width”.

### 2.2.5. Tension Stiffening Modeling

As already demonstrated for the cases of unconditioned RAC elements (Rangel et al. [42]), the numerical simulation of the experimental results obtained herein allowed to propose a comprehensive analysis of the steel rebar-concrete behavior. Based on the finite difference method proposed by Soranakom & Mobasher [43], it was possible to model the tension stiffening load-strain curves in order to indirectly identify the steel-to-concrete bond-slip law. In addition, this modeling approach allowed the analysis of the cracks' formation and propagation as well as the contribution of the isolated concrete matrix in reinforced RAC elements after being submitted to multiple freeze-thaw and wet-dry cycles.

## 3. Results and Discussion

### 3.1. Effects of Freeze-Thaw and Wet-Dry Aging on Main Properties of Reinforced RAC Elements

Figure 4a proposes a schematic representation of the typical load-strain curve for reinforced concrete element and the isolated matrix contribution during the tension stiffening test. The figure also highlights the main parameters ( $E_{pre}$ ,  $E_{post}$ ,  $F_{1st}$ ,  $F_{yield}$ ,  $\epsilon_{1st}$ ,  $\epsilon_{final}$ ,  $C_1$ ,  $C_n$ ,  $f_{m,1st}$  and  $f_{m,final}$ ) that will be considered for the analysis of the experimental results. The reinforced concrete elements subjected to tension stiffening tests behave in accordance with the well-known ACK model [44], characterized by the following four phases: (i) Pre-cracking elastic phase; (ii) Multiple crack formation; (iii) Stabilized crack phase (post-cracking); and (iv) Yielding of reinforcement. On the other hand, Figure 4b,c present the curves obtained for the reference natural mixtures, confirming the above-described trend. The curves plotted in Figure 4b,c show an improvement (higher loads for the same strain) in the behavior of non-degraded REF(FT300) in comparison with the companion REF(FT150), which is explained by the higher cement hydration degree of older REF(FT300) samples. As a general trend, all mixtures presented a reduction in the load-strain behavior after degradation processes as for the same strain level, but the non-degraded samples reached higher strength values than the degraded ones (see Figure 4b).

The main representative parameters (and the corresponding coefficients of variation expressed in percentage) for the tested reinforced concrete elements subjected to freeze-thaw and wet-dry cycles are presented in Tables 3 and 4, respectively.

Until the appearance of the first crack (phase I in Figure 4a), since the composite is in the elastic phase, the load-strain curve slope is governed by the pre-cracking elastic modulus of the composite ( $E_{pre}$ ): the results show that for unconditioned elements, the presence of RCAs did not significantly influence this property. For instance, the values obtained for REF(FT150) of mixtures C35-NAT, C35-L-C1 and C35-D-C1 are equal to 25.8, 26.1 and 25.5 GPa, respectively. On the other hand, all tested mixtures presented elastic modulus reduction when undergoing degradation cycles. The highest degradation impact in both cases (300 freeze-thaw and 50 wet-dry cycles) was observed in the mixtures with the highest amount of attached mortar (i.e., RCA\_L\_C1). This behavior is related with the higher values of concrete open porosity (see Table 2) that allows an easier flow of water into the concrete element. For example, the mixtures subjected to 150 freeze-thaw cycles (Table 3) suffered decreases in the elastic modulus in the range of 6% (from 5.4% to 6.2%) in relation to the non-degraded references. The damage was more pronounced when the samples were submitted to 300 cycles. The modulus reduction reached 16% for the C35-NAT mixture and 22% for the C35-L-C1 concrete. After wet-dry cycles, the elastic modulus of the tension stiffening elements submitted to 25 cycles was only slightly decreased (3.0% to 5.5% (see Table 4). After 50 cycles, the elastic modulus of C35-NAT and C35-L-C1 mixtures was reduced by about 10% and 16%, respectively.

The multiple crack formation (phase II in Figure 4a) begins at the moment of the appearance of the first crack, and at that moment the first crack strength ( $f_{1st}$ ) and strain ( $\epsilon_{1st}$ ) were determined. For the lower level of degradation (i.e., 150 freeze-thaw and 25 wet-dry cycles), the higher porosity of the RCAs does not seem to have affected the composite response.

Conversely, for higher number of cycles, the presence of a more porous aggregate caused a slightly higher reduction in the first crack strength of the degraded elements. For example, after 150 freeze-thaw cycles (Table 3) the percentage drop in first-crack values for the three concrete mixtures ranged from 5.0% to 6.5%. After 300 cycles, however, the  $f_{1st}$  decreased by about 13.0% for C35-NAT, 16.0% for C35-D-C1 and 18.0% for C35-L-C1.

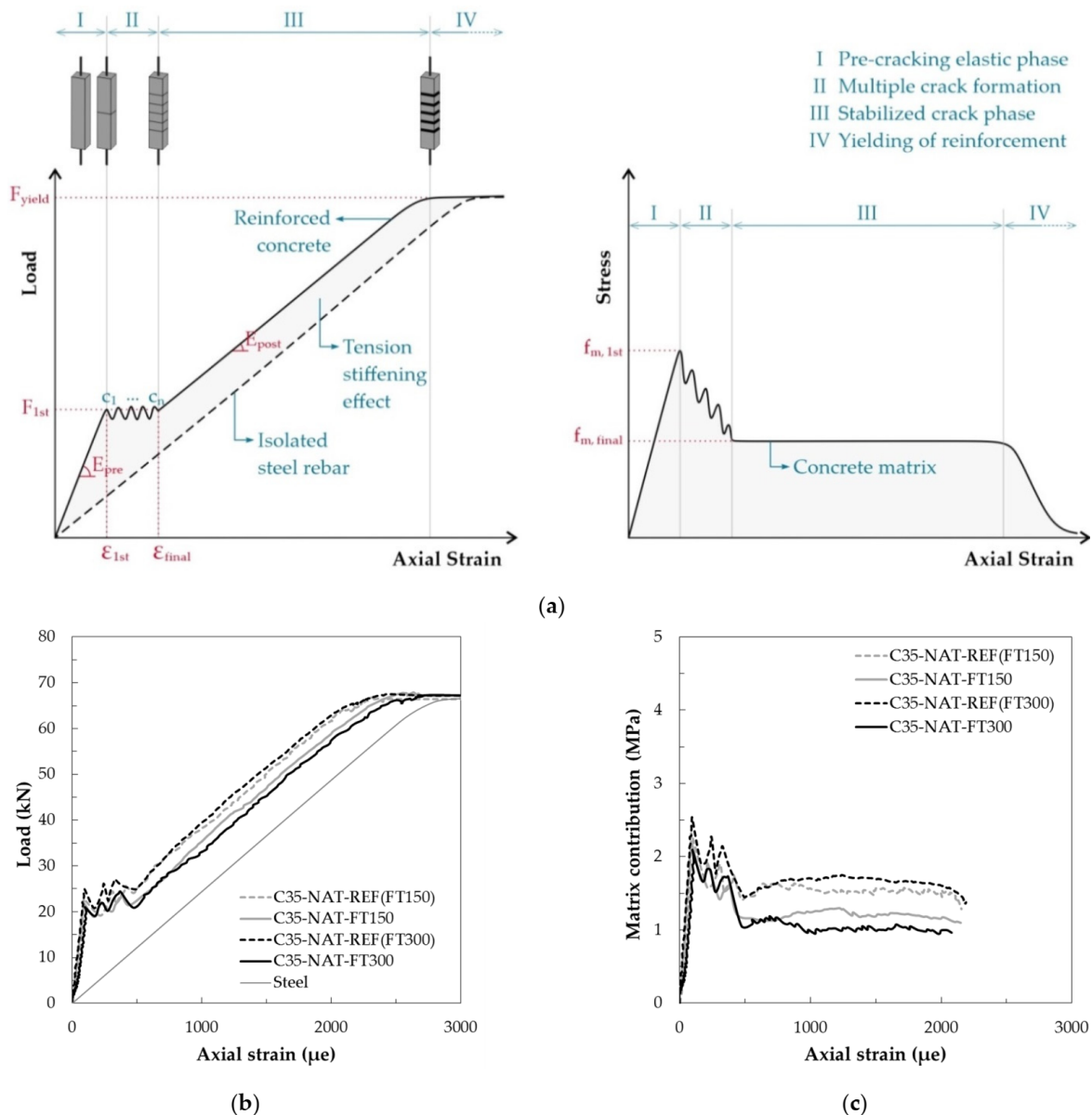


**Figure 4.** (a) Schematic description of the typical behaviors of the reinforced concrete and the isolated matrix contribution in the tension stiffening test with the indication of the main analysis parameters; (b) Load-strain curve for NAT-concrete mixtures; (c) Matrix contribution on tension-stiffening test for NAT-concrete mixtures.



**Table 3.** Main representative parameters for tested reinforced elements subjected to freeze-thaw cycles.

| Mixtures | ID         | Pre-Cracking Phase |                    |                                       | Post-Cracking Phase                     |                     | Isolated Matrix      |                        |
|----------|------------|--------------------|--------------------|---------------------------------------|---|---------------------|----------------------|------------------------|
|          |            | $E_{pre}$<br>(GPa) | $f_{1st}$<br>(MPa) | $\epsilon_{1st}$<br>( $\mu\epsilon$ ) | $\epsilon_{final}$<br>( $\mu\epsilon$ ) | $E_{post}$<br>(GPa) | $f_{m,1st}$<br>(MPa) | $f_{m,final}$<br>(MPa) |
| C35-NAT  | REF(FT150) | 25.8 (2.0)         | 2.54 (1.6)         | 89 (1.0)                              | 486 (11.0)                              | 2.71 (1.6)          | 2.34 (1.8)           | 1.40 (1.7)             |
|          | FT150      | 24.2 (1.1)         | 2.41 (0.6)         | 90 (0.6)                              | 432 (4.5)                               | 2.65 (4.1)          | 2.20 (0.8)           | 1.24 (2.0)             |
|          | REF(FT300) | 26.3 (1.0)         | 2.70 (1.7)         | 93 (2.3)                              | 467 (6.2)                               | 2.67 (1.8)          | 2.48 (1.7)           | 1.40 (4.2)             |
|          | FT300      | 22.2 (4.4)         | 2.34 (0.8)         | 96 (4.4)                              | 491 (6.3)                               | 2.72 (3.0)          | 2.11 (0.9)           | 1.13 (6.9)             |
| C35-L-C1 | REF(FT150) | 26.1 (0.3)         | 2.88 (0.9)         | 99 (1.1)                              | 469 (12.3)                              | 2.48 (4.2)          | 2.65 (0.9)           | 1.57 (6.4)             |
|          | FT150      | 24.6 (1.0)         | 2.69 (0.9)         | 99 (1.9)                              | 470 (4.2)                               | 2.65 (3.6)          | 2.46 (0.6)           | 1.29 (2.9)             |
|          | REF(FT300) | 26.7 (2.4)         | 2.98 (0.4)         | 101 (2.9)                             | 517 (6.1)                               | 2.67 (1.8)          | 2.76 (0.4)           | 1.59 (2.4)             |
|          | FT300      | 20.8 (2.4)         | 2.44 (0.8)         | 106 (2.3)                             | 540 (9.5)                               | 2.54 (3.5)          | 2.19 (0.9)           | 1.07 (8.5)             |
| C35-D-C1 | REF(FT150) | 25.5 (2.7)         | 2.71 (2.2)         | 96 (0.7)                              | 480 (4.7)                               | 2.49 (4.0)          | 2.49 (2.4)           | 1.54 (2.0)             |
|          | FT150      | 24.1 (1.1)         | 2.58 (1.6)         | 97 (0.9)                              | 458 (3.7)                               | 2.81 (1.7)          | 2.35 (1.7)           | 1.29 (2.1)             |
|          | REF(FT300) | 26.5 (4.0)         | 2.80 (0.7)         | 95 (3.5)                              | 507 (11.7)                              | 2.63 (5.6)          | 2.58 (1.0)           | 1.61 (6.9)             |
|          | FT300      | 21.7 (2.8)         | 2.36 (1.8)         | 98 (3.7)                              | 456 (10.9)                              | 2.67 (1.6)          | 2.12 (1.8)           | 1.13 (2.1)             |

**Table 4.** Main representative parameters for tested reinforced elements subjected to wet-dry cycles.

| Mixtures | ID        | Pre-Cracking Phase |                    |                                       | Post-Cracking Phase                     |                     | Isolated Matrix      |                        |
|----------|-----------|--------------------|--------------------|---------------------------------------|---|---------------------|----------------------|------------------------|
|          |           | $E_{pre}$<br>(GPa) | $f_{1st}$<br>(MPa) | $\epsilon_{1st}$<br>( $\mu\epsilon$ ) | $\epsilon_{final}$<br>( $\mu\epsilon$ ) | $E_{post}$<br>(GPa) | $f_{m,1st}$<br>(MPa) | $f_{m,final}$<br>(MPa) |
| C35-NAT  | REF(WD25) | 25.8 (2.0)         | 2.54 (1.6)         | 89 (1.0)                              | 486 (11.0)                              | 2.71 (1.6)          | 2.34 (1.8)           | 1.40 (1.7)             |
|          | WD25      | 25.0 (1.4)         | 2.49 (1.3)         | 90 (2.6)                              | 466 (6.8)                               | 2.59 (2.9)          | 2.28 (1.2)           | 1.31 (3.2)             |
|          | REF(WD50) | 26.3 (1.0)         | 2.70 (1.7)         | 93 (2.3)                              | 467 (6.2)                               | 2.67 (1.8)          | 2.48 (1.7)           | 1.40 (4.2)             |
|          | WD50      | 23.5 (2.5)         | 2.44 (2.7)         | 94 (0.6)                              | 479 (7.7)                               | 2.69 (5.2)          | 2.22 (2.9)           | 1.23 (3.9)             |
| C35-L-C1 | REF(WD25) | 26.1 (0.3)         | 2.88 (0.9)         | 99 (1.1)                              | 469 (12.3)                              | 2.48 (4.2)          | 2.65 (0.9)           | 1.57 (6.4)             |
|          | WD25      | 24.7 (0.7)         | 2.74 (0.6)         | 100 (1.2)                             | 507 (8.0)                               | 2.76 (3.7)          | 2.51 (0.6)           | 1.37 (7.6)             |
|          | REF(WD50) | 26.7 (2.4)         | 2.98 (0.4)         | 101 (2.9)                             | 517 (6.1)                               | 2.67 (1.8)          | 2.76 (0.4)           | 1.59 (2.4)             |
|          | WD50      | 22.3 (2.6)         | 2.54 (3.9)         | 103 (6.0)                             | 481 (4.1)                               | 2.62 (8.1)          | 2.30 (4.3)           | 1.19 (2.5)             |
| C35-D-C1 | REF(WD25) | 25.5 (2.7)         | 2.71 (2.2)         | 96 (0.7)                              | 480 (4.7)                               | 2.49 (4.0)          | 2.49 (2.4)           | 1.54 (2.0)             |
|          | WD25      | 24.4 (1.8)         | 2.62 (2.7)         | 97 (4.5)                              | 494 (5.2)                               | 2.67 (2.5)          | 2.40 (2.6)           | 1.37 (7.5)             |
|          | REF(WD50) | 26.5 (4.0)         | 2.80 (0.7)         | 95 (3.5)                              | 507 (11.7)                              | 2.63 (5.6)          | 2.58 (1.0)           | 1.61 (6.9)             |
|          | WD50      | 23.1 (0.5)         | 2.48 (1.7)         | 97 (2.2)                              | 454 (3.4)                               | 2.83 (3.1)          | 2.25 (1.6)           | 1.26 (2.8)             |

The same trend was observed for the samples submitted to wet-dry cycles (see Table 4). The decreases in first crack strength for C35-NAT element increased from 2.1% to 9.6% when the number of cycles was augmented from 25 for 50 cycles. The values observed for the NAT-concrete samples were, however, lower than the results obtained for concretes with RCAs: C35-L-C1 registered a 4.7% drop in first crack strength after 25 cycles of wet-dry and 15% for 50 cycles, whereas C35-D-C1 achieved reductions of 3.2% and 11.6% for 25 and 50 cycles, respectively.

The first crack strain ( $\epsilon_{1st}$ ) obtained for the natural mixture was slightly smaller than the values obtained for the RCAs. For instance, C35-NAT presented the first crack at 89  $\mu\epsilon$ , while for C35-D-C1 and C35-L-C1 values were 99  $\mu\epsilon$  and 96  $\mu\epsilon$ , respectively. It was observed that, for the highest levels of degradation, all three mixtures showed an increase in this parameter what is in accordance with the discussion made for the elastic modulus of the mixtures. This can be highlighted by looking at REF(FT300) and FT300 values of C35-L-C1 mixture, which ranged from 101  $\mu\epsilon$  to 106  $\mu\epsilon$ .

After the first crack, as the tensile load continued to be applied, more cracks appeared in the concrete ( $C_2, \dots, C_n$ ), until the matrix was divided into several segments. At this moment, the final post-cracking strain ( $\epsilon_{final}$ ) was identified in the composite load-strain curve. The difference between the values of  $\epsilon_{final}$  and  $\epsilon_{1st}$  determines the length of multiple cracking phase. The experimentally obtained values of  $\epsilon_{final}$  are in the range of 500  $\mu\epsilon$  for

non-aged and aged specimens (Tables 3 and 4). No relationship was identified between the types of aggregates and the deformation length of the cracking process phase.

As expected, the post-cracking elastic modulus of the composite ( $E_{\text{post}}$ ) approaches the elastic modulus of the steel rebar. The tension stiffening effect was evaluated by isolating the contribution of the concrete matrix from the composite force-strain diagram. The matrix stress-strain curve is defined by the opening of the first crack, marking the matrix strength to the first crack,  $f_{m,1st}$ . In non-degraded mixes, the highest matrix strength was obtained for C35-L-C1, followed by C35-D-C1. As this property of the composite is directly related to the tensile strength of the matrix, these results are in agreement with the values shown in Table 2, since C35-L-C1 also presented the highest value of  $f_{t,28}$ . After both types of aging, the C35-L-C1 is the mixture that suffered the highest deterioration in  $f_{m,1st}$  and this can be explained by its greater amount of total mortar and, consequently, the higher porosity of this matrix.

Once the multiple cracking phase is completed, the stage determined by widening of the cracks to an approximately constant stress begins (phase III) and the final post-cracking matrix strength ( $f_{m,final}$ ) is achieved. This parameter was reduced by about 30% and 33% for mixtures C35-D-C1 and C35-L-C1, respectively, after 300 freezing and thawing cycles, compared to a reduction of about 19% for NAT-concrete (see Table 3). A similar trend was observed also in the case of samples submitted to the wet-dry cycles.

### 3.2. Effects of Freeze-Thaw and Wet-Dry Aging on Cracking Process of Reinforced RAC Elements

The transverse cracking process during the tests presents a typical pattern of four to five cracks, and this pattern is in agreement with force discontinuities recorded in cracking stage of load-strain curves (Figure 4b). The creation and propagation of cracks for each mixture and each level of aging were analyzed in relation to crack spacing and crack width (see Figure 5). Crack spacing values were determined at a strain of about  $500 \mu\epsilon$ , which in the present study ensure the end of the multiple crack process for all mixtures (see values of  $\epsilon_{\text{final}}$  in Tables 3 and 4). In addition, the final crack width values at the strain of  $2500 \mu\epsilon$  were also measured, corresponding to the point in which the concrete matrix contribution ended.

The results showed that, among the non-degraded mixtures, C35-D-C1 presented the lowest values for crack spacing, mostly for advanced ages (Figure 5a,b). For both C35-NAT and C35-L-C1, with the increase of cycles, crack spacing values decreased, indicating an “earlier” crack opening process; and this loss in resistance to aging was most prominent for the recycled one. For C35-D-C1, the degradation processes did not significantly influence the cracking spacing, where the values varied from 129 mm to 126 mm, when the number of freeze-thaw cycles increased from 150 to 300. The same behavior was observed for the increase of wet-dry cycles.

As the deformation of the reinforced element increases, the average crack width increases along the multiple crack stage, even with the creation of new cracks, and then, after the element reaches the maximum number of cracks, it continues to increase with a higher rate. For non-degraded mixtures, crack width was greater for mixtures containing RCA and this became more evident with advancing age. More specifically, for C35-NAT, the crack opening value was of 1.27 mm, while for RAC mixtures this property reached values of 1.34 mm and 1.41 mm for both C35-L-C1 and C35-D-C1, respectively. As the number of cycles increases, the crack width value increases. As a general trend, the largest openings throughout the test were found for C35-D-C1 samples in both degradation tests (Figure 5c,d).

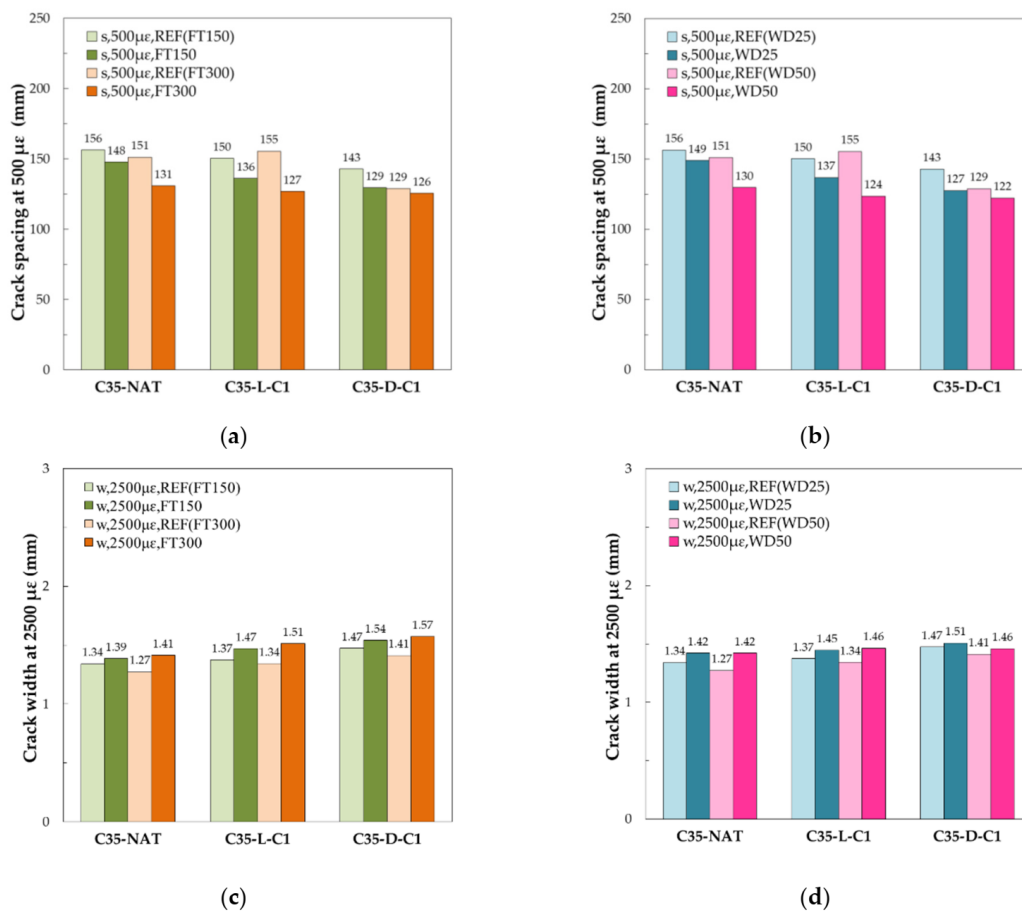


**Figure 5.** Main properties of crack analysis in the freeze-thaw and wet-dry durability studies: (a,b) Initial crack spacing (at 500 με); (c,d) Final crack width (at 2500 με).

### 3.3. Effects of Freeze-Thaw and Wet-Dry Aging on Bond Behavior of Reinforced RAC Elements

As already mentioned, the experimental results of the tension stiffening elements were simulated using a finite difference method in order to estimate the steel-to-concrete bond-slip law strength ( $\tau_b$  in Table 5).

**Table 5.** Effects of freeze-thaw and wet-dry aging on bond strength of reinforced RAC.

| Mixtures | ID         | $\tau_b$ (MPa) | ID        | $\tau_b$ (MPa) |
|----------|------------|----------------|-----------|----------------|
| C35-NAT  | REF(FT150) | 17.4           | REF(WD25) | 17.4           |
|          | FT150      | 16.5           | WD25      | 16.7           |
|          | REF(FT300) | 17.9           | REF(WD50) | 17.9           |
|          | FT300      | 16.0           | WD50      | 16.5           |
| C35-L-C1 | REF(FT150) | 16.1           | REF(WD25) | 16.1           |
|          | FT150      | 15.2           | WD25      | 15.3           |
|          | REF(FT300) | 16.6           | REF(WD50) | 16.6           |
|          | FT300      | 14.1           | WD50      | 14.7           |
| C35-D-C1 | REF(FT150) | 16.7           | REF(WD25) | 16.7           |
|          | FT150      | 15.7           | WD25      | 16.0           |
|          | REF(FT300) | 17.1           | REF(WD50) | 17.1           |
|          | FT300      | 14.7           | WD50      | 15.2           |

In the non-degraded samples, it was observed that the higher the amount of attached mortar to the aggregate, the lower the value of the bond strength. For example, for REF(FT150), the natural concrete achieved a  $\tau_b$  value equal to 17.4 MPa, while the recycled

mixtures registered lower values equal to 16.7 and 16.1 MPa (C35-D-C1 and C35-L-C1, respectively). As expected, the results showed that this property is directly influenced by the hydration time. For C35-NAT mixture, the  $\tau_b$  increased from 17.4 to 17.9 MPa and similar trend was observed for mixtures with recycled aggregates.

Regarding the degradation processes, up to 150 freeze-thaw cycles, the natural and recycled mixtures appear to behave in the same way, reaching similar decrease values from 5.2% to 6.2%. However, by increasing the level of aging up to 300 cycles, the rate of drop in bond increases for recycled concrete, while the natural mixture maintains the same rate. Consequently, at the end of 300 cycles, C35-NAT was represented by a smaller decrease of 10.9%, while the concrete produced with RCA from demolition waste reached 14.0% and the concrete produced with RCA from laboratory waste reached the highest impact of 14.8%.

Therefore, the presence of RCAs in concrete promotes a greater impact on the steel-concrete bond performance of structural elements after degradation processes than for concrete produced with only natural aggregate.

#### 4. Freeze-Thaw and Wet-Dry Degradation-Law for Reinforced RAC

With the experimental results obtained for the structural properties discussed above, a generalized degradation-law is proposed for reinforced RAC subjected to freeze-thaw aging or wet-dry aging: the law represents the relationships between an initial property of the isolated intact concrete, in this case, the concrete water absorption capacity, herein defined as concrete open porosity ( $w_{open}$ ), and the variations obtained in the main structural properties of the steel-concrete composite after freeze-thaw or wet-dry degradation, that is, pre-cracking elastic modulus ( $E_{pre}$ ), first crack load ( $F_{1st}$ ) and bond strength ( $\tau_b$ ). The three proposed relationships are described in the following equations:

$$\frac{E_{pre,AGING}}{E_{pre,REF}} = \frac{1}{1 + a^2 \cdot w_{open}} \quad (2)$$

$$\frac{F_{1st,AGING}}{F_{1st,REF}} = \frac{1}{1 + b^2 \cdot w_{open}} \quad (3)$$

$$\frac{\tau_{b,AGING}}{\tau_{b,REF}} = \frac{1}{1 + c^2 \cdot w_{open}} \quad (4)$$

where  $a$ ,  $b$  and  $c$  are calibrated parameters in relation to each of the structural properties: pre-cracking elastic modulus, first crack load and bond strength, respectively. Figure 6 presents the calibrated degradation-law curves proposed by Equations (2) and (3) and the experimental results after freeze-thaw or wet-dry degradation.

The proposed degradation-law equations have physical significance and indicate that the degradation effect, expressed by the relation between the results obtained after each degradation scenario and the reference values, can be presented as a function of the initial open porosity of the concrete for each structural property of the composite. Hypothetically, if concrete were completely impermeable, that is, open porosity equal to zero, according to Equations (2)–(4), pre-cracking elastic modulus, first crack load and bond strength would not be affected by the aging effect.

From the results plotted (Figure 6), it is possible to observe that, in each group, the point with the lowest open porosity represents the reinforced natural concrete composite, while the others correspond to reinforced RAC composites. Due to their higher total mortar volume (as consequence of the presence of AM), steel-RAC elements have higher values of open porosity compared to steel-concrete elements without RCA incorporation.

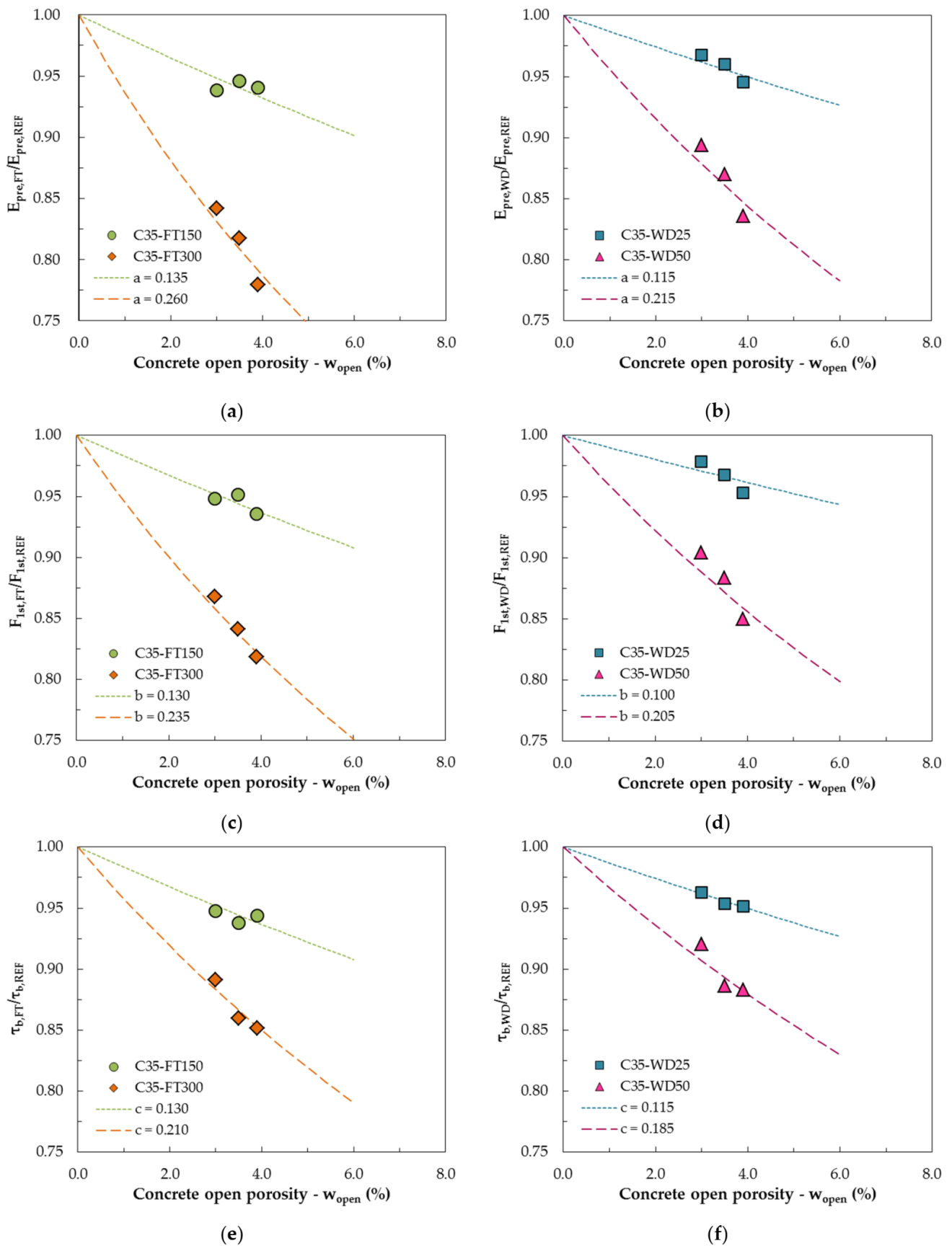


**Figure 6.** Relation between concrete open porosity and structural properties in the freeze-thaw and wet-dry durability studies: (a,b) Pre-cracking elastic modulus; (c,d) First crack load; (e,f) Bond strength.

It is worth mentioning that the proposed laws (see Equations (2)–(4)) state that concrete degradation is directly related to the initial open porosity of the concrete ( $w_{open}$ ), which is directly related (see Equation (1)) to the total volume of mortar ( $V_{M,tot}$  in Table 2) and, consequently, to the “quality” (considering the amount of attached mortar,  $V_{AM}$  in Table 1, characterizing the employed recycled particles) and amount of RCAs.

For both freeze-thaw and wet-dry aging, the smaller number of cycles (represented by the top points) did not cause significant reductions in the structural properties of the composites after degradation. However, the degradation effect is more evident in the lower points, which represent the samples that have undergone the greatest number of cycles.

The more horizontal shape of the curves corresponding to the smaller number of cycles shows that, even by increasing the open porosity, the structural properties have been little changed. This means that, for a lower degradation level, the presence of recycled aggregates does not significantly influence the composite’s degradation. On the other hand, the highest degradation level curves present a greater slope, which makes the structural properties of the composite more sensitive to the concrete open porosity increase. Thus, small variations in this initial concrete property provide a greater reduction in pre-cracking elastic modulus, first crack load and bond strength after 50 wet-dry cycles and 300 freeze-thaw cycles.

It is worth emphasizing that, despite being higher than in composites without RCA incorporation, the degradation effect on the structural performance of steel-RAC composites is relatively low.

In brief, from the proposed degradation-law, it is possible to affirm that the initial open porosity of concrete is the key to predict the degradation effects on structural durability of steel-RAC elements. As open porosity is related to the total mortar volume and, consequently, to the mortar content of the recycled aggregate, the solution to guarantee the use of RAC in structures exposed to external agents is to control this property in the concrete mix-design.

## 5. Conclusions

The present study reports on an analysis of the structural performance of reinforced concrete elements after degradation processes. Specifically, it summarizes the results of an experimental investigation aimed at analyzing the tension stiffening behavior of steel-concrete composites, of normal strength concretes containing RCAs with different attached mortar contents, after being separately undergone to freeze-thaw and wet-dry cycles. According to the obtained results, the following considerations can be highlighted for both aging processes:

- The degraded elements’ curves presented lower values of strength for both the multiple cracking phase and post cracking phase than the curves of the non-degraded elements. However, after degradation, all composites still present the standard behavior of the tension stiffening test, with the four well-defined phases;
- In the elastic phase, the results show that the presence of RCAs did not significantly influence the elastic modulus of non-degraded samples;
- Both elastic modulus and first crack strength were more impacted by the degradation processes in the concrete with the highest amount of attached mortar in its aggregate. This impact is caused by the greater flow of water and aggressive agents inside the concrete, provided by its greater porosity;
- All mixtures showed a reduction in the stress-strain performance of insulated concrete after degradation. Specifically, the attached mortar content also directly impacted the maximum strength of the concrete matrix;
- The presence of RCAs does not interfere with the cracking pattern of concrete submitted to the aging processes of this study. The spacing behavior was similar for reference and degraded samples. In general, the largest crack openings throughout the test were verified for samples subjected to higher levels of degradation;

- A degradation law relating the aging effect to the open porosity of concrete was developed for both degradation processes—freeze-thaw and wet-dry cycles. Regardless of the aggregate origin, for higher degradation degrees, the total mortar volume in the concrete is the main property for understanding the cycles effects on structural performance. The higher total mortar volume in the concrete composition (and, consequently, the higher concrete water absorption), the higher the impact that degradation will have on the following structural properties: pre-cracking elastic modulus, first crack composite strength, first crack matrix strength, final post-cracking matrix strength and, finally, steel-concrete bond strength;
- The feasibility of using recycled aggregates in structural elements exposed to aggressive external agents can be guaranteed as long as the open porosity is properly considered in the concrete mix-design: this is, certainly, possible if a fundamental characterization of the raw materials is performed (e.g., evaluation of the Attached Mortar content in RCA) and, moreover, a specific mixture proportioning method is used for the RAC (e.g., using the Compressible Packing Method proposed herein).

**Author Contributions:** Conceptualization, M.P., E.M. and R.D.T.F.; methodology, C.S.R. and M.A.; validation, C.S.R., M.P., M.A. and L.C.M.; formal analysis, C.S.R. and M.P.; investigation, C.S.R. and M.A.; resources, R.D.T.F.; data curation, C.S.R., M.P. and L.C.M.; writing—original draft preparation, C.S.R.; writing—review and editing, M.P., M.A., L.C.M., E.M. and R.D.T.F.; visualization, C.S.R. and M.P.; supervision, M.P., E.M. and R.D.T.F.; project administration, R.D.T.F.; funding acquisition, R.D.T.F. All authors have read and agreed to the published version of the manuscript.

**Funding:** This study was financed in part by the Coordenação de Aperfeiçoamento de Pessoal de Nível Superior—Brasil (CAPES)—Finance Code 001. This work was carried out with support from CNPq, Conselho Nacional de Desenvolvimento Científico e Tecnológico—Brasil. The present research is also part of the activities carried out by the second Author (M.P.) within a post-doctoral project co-funded by the Department of Civil Engineering of University of Salerno (Italy) and COPPETEC foundation (UFRJ, Brazil).

**Acknowledgments:** The present study is part of the activities carried out by the Authors within the “SUPERCONCRETE” Project ([www.superconcrete-h2020.unisa.it](http://www.superconcrete-h2020.unisa.it)) (access on 23 September 2021) funded by the European Union within the Horizon 2020 Framework Programme (H2020-MSCA-RISE-2014 No. 645704).

**Conflicts of Interest:** The authors declare no conflict of interest.

## References

1. Fiol, F.; Thomas, C.; Manso, J.M.; López, I. Influence of Recycled Precast Concrete Aggregate on Durability of Concrete’s Physical Processes. *Appl. Sci.* **2020**, *10*, 7348. [[CrossRef](#)]
2. Barroqueiro, T.; da Silva, P.R.; de Brito, J. High-Performance Self-Compacting Concrete with Recycled Aggregates from the Precast Industry: Durability Assessment. *Buildings* **2020**, *10*, 113. [[CrossRef](#)]
3. Liu, H.; Hua, M.; Zhu, P.; Chen, C.; Wang, X.; Qian, Z.; Dong, Y. Effect of Freeze–Thaw Cycles on Carbonation Behavior of Three Generations of Repeatedly Recycled Aggregate Concrete. *Appl. Sci.* **2021**, *11*, 2643. [[CrossRef](#)]
4. Verian, K.P.; Ashraf, W.; Cao, Y. Properties of recycled concrete aggregate and their influence in new concrete production. *Resour. Conserv. Recycl.* **2018**, *133*, 30–49. [[CrossRef](#)]
5. Ouyang, K.; Shi, C.; Chu, H.; Guo, H.; Song, B.; Ding, Y.; Guan, X.; Zhu, J.; Zhang, H.; Wang, Y.; et al. An overview on the efficiency of different pretreatment techniques for recycled concrete aggregate. *J. Clean. Prod.* **2020**, 263. [[CrossRef](#)]
6. Pani, L.; Francesconi, L.; Rombi, J.; Mistretta, F.; Sassu, M.; Stochino, F. Effect of Parent Concrete on the Performance of Recycled Aggregate Concrete. *Sustainability* **2020**, *12*, 9399. [[CrossRef](#)]
7. Amario, M.; Rangel, C.S.; Pepe, M.; Toledo Filho, R.D. Optimization of normal and high strength recycled aggregate concrete mixtures by using packing model. *Cem. Concr. Compos.* **2017**, *84*, 83–92. [[CrossRef](#)]
8. Muduli, R.; Mukharjee, B.B. Performance assessment of concrete incorporating recycled coarse aggregates and metakaolin: A systematic approach. *Constr. Build. Mater.* **2020**, *233*, 117223. [[CrossRef](#)]
9. Sadati, S.; Khayat, K.H. Can Concrete Containing High-Volume Recycled Concrete Aggregate Be Durable? *ACI Mater. J.* **2018**, *115*, 471–480. [[CrossRef](#)]
10. Shang, H.; Song, Y.; Ou, J. Behavior of air-entrained concrete after freeze-thaw cycles. *Acta Mech. Solida Sin.* **2009**, *22*, 261–266. [[CrossRef](#)]

11. Liu, Y.; Chen, Y.F.; Wang, W.; Li, Z. Bond performance of thermal insulation concrete under freeze–thaw cycles. *Constr. Build. Mater.* **2016**, *104*, 116–125. [[CrossRef](#)]
12. Liu, K.; Yan, J.; Meng, X.; Zou, C. Bond behavior between deformed steel bars and recycled aggregate concrete after freeze–thaw cycles. *Constr. Build. Mater.* **2020**, *232*, 117236. [[CrossRef](#)]
13. Thomas, R.J.; Fellows, A.J.; Sorensen, A.D. Durability analysis of recycled asphalt pavement as partial coarse aggregate replacement in a high-strength concrete mixture. *J. Mater. Civ. Eng.* **2018**, *30*, 04018061. [[CrossRef](#)]
14. Bassani, M.; Tefa, L. Compaction and freeze–thaw degradation assessment of recycled aggregates from unseparated construction and demolition waste. *Constr. Build. Mater.* **2018**, *160*, 180–195. [[CrossRef](#)]
15. Kazmi, S.M.S.; Munir, M.J.; Wu, Y.F.; Patnaikuni, I.; Zhou, Y.; Xing, F. Effect of different aggregate treatment techniques on the freeze–thaw and sulfate resistance of recycled aggregate concrete. *Cold Reg. Sci. Technol.* **2020**, *178*, 103126. [[CrossRef](#)]
16. Lu, C.; Zhou, Q.; Wang, W.; Wei, S.; Wang, C. Freeze–thaw resistance of recycled aggregate concrete damaged by simulated acid rain. *J. Clean. Prod.* **2021**, *280*, 124396. [[CrossRef](#)]
17. Rangel, C.S.; Amario, M.; Pepe, M.; Martinelli, E.; Toledo Filho, R.D. Durability of Structural Recycled Aggregate Concrete Subjected to Freeze–Thaw Cycles. *Sustainability* **2020**, *12*, 6475. [[CrossRef](#)]
18. Ren, G.; Shang, H.; Zhang, P.; Zhao, T. Bond behaviour of reinforced recycled concrete after rapid freezing–thawing cycles. *Cold. Reg. Sci. Technol.* **2019**, *157*, 133–138. [[CrossRef](#)]
19. Shang, H.S.; Zhao, T.J.; Cao, W.Q. Bond behavior between steel bar and recycled aggregate concrete after freeze–thaw cycles. *Cold. Reg. Sci. Technol.* **2015**, *118*, 38–44. [[CrossRef](#)]
20. Huaishuai, S.; Zhiheng, W.; Peng, Z.; Tiejun, Z.; Guoxi, F.; Guosheng, R. Bond behavior of steel bar in air-entrained RCAC in fresh water and sea water after fast freeze–thaw cycles. *Cold. Reg. Sci. Technol.* **2017**, *135*, 90–96. [[CrossRef](#)]
21. Wu, Z.; Wong, H.S.; Buenfeld, N.R. Transport properties of concrete after drying–wetting regimes to elucidate the effects of moisture content, hysteresis and microcracking. *Cem. Concr. Res.* **2017**, *98*, 136–154. [[CrossRef](#)]
22. Rangel, C.S.; Amario, M.; Pepe, M.; Martinelli, E.; Toledo Filho, R.D. Influence of Wetting and Drying Cycles on Physical and Mechanical Behavior of Recycled Aggregate Concrete. *Materials* **2020**, *13*, 5675. [[CrossRef](#)] [[PubMed](#)]
23. Rangel, C.S.; Toledo Filho, R.D.; Amario, M.; Pepe, M.; de Castro Polisseni, G.; de Andrade, G.P. Generalized quality control parameter for heterogenous recycled concrete aggregates: A pilot scale case study. *J. Clean. Prod.* **2019**, *208*, 589–601. [[CrossRef](#)]
24. ABNT NBR 16916. *Fine Aggregate—Determination of Density and Water Absorption*; Associação Brasileira de Normas Técnicas: Rio de Janeiro, Brazil, 2021.
25. ABNT NBR NM 53. *Coarse Aggregate—Determination of the Bulk Specific Gravity, Apparent Specific Gravity and Water Absorption*; Associação Brasileira de Normas Técnicas: Rio de Janeiro, Brazil, 2009.
26. ABNT NBR NM 51. *Small-Size Coarse Aggregate—Test Method for Resistance to Degradation by Los Angeles Machine*; Associação Brasileira de Normas Técnicas: Rio de Janeiro, Brazil, 2001.
27. ABNT NBR 16697. *Portland Cement—Requirements*; Associação Brasileira de Normas Técnicas: Rio de Janeiro, Brazil, 2018.
28. de Larrard, F. *Concrete Mixture Proportioning: A Scientific Approach*; Series: Modern Concrete Technology; CRC Press: London, UK, 1999.
29. Pepe, M.; Toledo Filho, R.D.; Koenders, E.A.; Martinelli, E. A novel mix design methodology for Recycled Aggregate Concrete. *Constr. Build. Mater.* **2016**, *122*, 362–372. [[CrossRef](#)]
30. Pepe, M.; Toledo Filho, R.D.; Koenders, E.A.; Martinelli, E. Alternative processing procedures for recycled aggregates in structural concrete. *Constr. Build. Mater.* **2014**, *69*, 124–132. [[CrossRef](#)]
31. ABNT NBR 9778. *Hardened Mortar and Concrete—Determination of Absorption, Voids and Specific Gravity*; Associação Brasileira de Normas Técnicas: Rio de Janeiro, Brazil, 2009.
32. ABNT NBR 5739. *Concrete-Compression Test of Cylindrical Specimens*; Associação Brasileira de Normas Técnicas: Rio de Janeiro, Brazil, 2018.
33. ABNT NBR 8522. *Concrete-Determination of Static Modulus of Elasticity and Deformation by Compression*; Associação Brasileira de Normas Técnicas: Rio de Janeiro, Brazil, 2017.
34. ABNT NBR 7222. *Concrete and Mortar—Determination of the Tension Strength by Diametrical Compression of Cylindrical Test Specimens*; Associação Brasileira de Normas Técnicas: Rio de Janeiro, Brazil, 2011.
35. ABNT NBR 6892-1. *Metallic Materials-Tensile Testing Part 1: Method of Test at Room Temperature*; Associação Brasileira de Normas Técnicas: Rio de Janeiro, Brazil, 2018.
36. Tam, V.W.; Gao, X.F.; Tam, C.M. Microstructural analysis of recycled aggregate concrete produced from two-stage mixing approach. *Cem. Concr. Res.* **2005**, *35*, 1195–1203. [[CrossRef](#)]
37. Tam, V.W.; Tam, C.M. Assessment of durability of recycled aggregate concrete produced by two-stage mixing approach. *J. Mater. Sci.* **2007**, *42*, 3592–3602. [[CrossRef](#)]
38. ASTM C666. *Resistance of Concrete to Rapid Freezing and Thawing*; American Society for Testing and Materials: West Conshohocken, PA, USA, 2008.
39. ABNT NBR 13554. *Soil-Cement—Durability Test by Wetting and Drying-Test Method*; Associação Brasileira de Normas Técnicas: Rio de Janeiro, Brazil, 2012.
40. ASTM D559. *Standard Test Methods for Wetting and Drying Compacted Soil-Cement Mixtures*; American Society for Testing and Material: West Conshohocken, PA, USA, 2015.



41. ABNT NBR 7477. *Determinação do Coeficiente de Conformação Superficial de Barras e Fios de aço Destinados à Armadura de Concreto Armado*; Associação Brasileira de Normas Técnicas: São Paulo, Brazil, 1982. (In Portuguese)
42. Rangel, C.S.; Amario, M.; Pepe, M.; Yao, Y.; Mobasher, B.; Toledo Filho, R.D. Tension stiffening approach for interface characterization in recycled aggregate concrete. *Cem. Concr. Compos.* **2017**, *82*, 176–189. [[CrossRef](#)]
43. Soranakom, C.; Mobasher, B. Modeling of tension stiffening in reinforced cement composites: Part I. Theoretical modeling. *Mater. Struct.* **2010**, *43*, 1217–1230. [[CrossRef](#)]
44. Aveston, J.; Cooper, G.A.; Kelly, A. The properties of fibre composites. In *Conference Proceedings, National Physical Laboratory*; IPC Science and Technology Press: Surrey, England, 1971; pp. 15–26.